Thermoelectric properties and investigations of low thermal conductivity in Ga-doped Cu_{2}GeSe_{3}

J. Y. Cho, X. Shi, J. R. Salvador, G. P. Meisner, J. Yang, H. Wang, A. A. Wereszczak, X. Zhou, and C. Uher

Phys. Rev. B **84**, 085207 — Published 25 August 2011

DOI: 10.1103/PhysRevB.84.085207

Thermoelectric Properties and investigations of low thermal conductivity in Ga-doped Cu_2GeSe_3

J.Y. Cho and X. Shi
Optimal Inc. Plymouth Township, MI 48170, USA

J.R. Salvador* and G.P. Meisner,
Chemical Sciences and Materials Systems Laboratory,
GM R&D Center, Warren, Michigan 48090, USA

J. Yang
Electrochemical Energy Research Laboratory,
GM R&D Center, Warren, Michigan 48090, USA

H. Wang and A.A. Wereszczak
Materials Science and Technology Division,
Oak Ridge National Laboratory, Oak Ridge,
Tennessee 37831, USA

X. Zhou and C. Uher
Department of Physics, University of Michigan,
Ann Arbor, Michigan 48109, USA

*To whom correspondence should be addressed:
E-mail address: james.salvador@gm.com
Telephone: 586-986-5383
Fax: 586-986-3091

ABSTRACT

In this study, we have synthesized a series of low thermal conductivity diamond-like materials with the general formula $Cu_2Ga_xGe_{1-x}Se_3$ for $0 \leq x \leq 0.1$, and their transport properties were evaluated to establish their suitability for TE based waste heat recovery applications. We report results for the Seebeck coefficient (S), electrical resistivity (ρ), thermal conductivity (κ), Hall coefficient (R_H), crystal structure, and elastic properties of $Cu_2Ga_xGe_{1-x}Se_3$ for x = 0.01, 0.03, 0.05, 0.07 and 0.1. Powder x-ray diffraction revealed that a small amount of a related cubic polymorph appeared along with the orthorhombic parent phase at high Ga concentrations. This cubic phase is related to the parent phase in that both contain three-dimensional tetrahedral diamond-like substructures. All samples showed positive values of S and R_H over the entire temperature range studied, indicative of p-type charge carriers. The largest value of $S = 446\ \mu VK^{-1}$ was observed at 745 K for undoped Cu_2GeSe_3. With increasing Ga content, both S and ρ decreased. Low values of κ were observed for all samples with the lowest value of $\kappa = 0.67\ W\ m^{-1}\ K^{-1}$ at 745 K for undoped Cu_2GeSe_3. This value approaches the theoretical minimum thermal conductivity for these materials at high temperatures. Although this diamond-like material has highly symmetric, lower coordination number tetrahedral bonding, an unusually large Grüneisen parameter (γ), a measure of bonding anharmonicity, was observed for $Cu_2Ga_{0.1}Ge_{0.9}Se_3$. A value of γ = 1.7 was calculated from the measured values of the elastic properties, heat capacity, and volume thermal expansion. Given the fact that all materials investigated have similar elastic property values and likely comparable coefficients of thermal expansion we surmise that this large Grüneisen parameter is a general feature for this material system. We conclude that this high level of anharmonicity gives rise to enhanced phonon-

phonon scattering that is, in addition to the scattering brought about by the disordered structure, resulting in very low values of thermal conductivity.

INTRODUCTION

The performance of thermoelectric (TE) materials has been significantly improved in recent years, and their importance for electrical power generation using waste heat recovery and for cooling using Peltier refrigeration has garnered significant interest due to the world's energy demand and concern for the environment.[1-3] The TE performance of a material is characterized by its dimensionless thermoelectric figure of merit $ZT = S^2T/\rho\kappa$, where S is the Seebeck coefficient, T the absolute temperature, ρ the electrical resistivity, and κ the total thermal conductivity. Great effort has been expended in materials research and optimization utilizing the concepts of phonon-glass electron-crystal compounds (PGEC),[4-6] nano-inclusion materials,[7,8] and investigating compounds with complex crystal structures [9,10] with the goal of achieving high ZT TE materials.

Diamond-like semiconductors, which are composed of tetrahedrally coordinated constituent elements, have recently gained interest in thermoelectrics due to their high TE performance. Liu *et al*. showed reasonable TE properties for the Cu based quaternary chalcogenide $Cu_2CdSnSe_4$, which has a low κ [11] that is thought to be due to structural disorder. For the wide band gap semiconductor system Cu_2ZnSnX_4 (X = S, Se), an exceptionally low κ at elevated temperatures also leads to good TE performance.[12,13] Interestingly, the small energy difference, based on first principle calculations, between polymorphs arising from substitutional disorder on the cation sites for Cu_2ZnSnX_4 (X = S, Se) has been reported as a possible reason for the further decrease of κ with increasing temperatures.[14]

Recently a new model has been proposed to explain the low thermal conductivity of the Cu_2SnSe_3 materials based on ab-initio band structure calculations. These calculations find that (1) the charge accumulation of the valence bands resides on the Cu-Se network, which therefore dominates the hole conduction, and (2) that Sn makes virtually no contribution to these bands,

which is therefore merely donating the proper number of electrons to the system to meet bonding requirements. The conclusion here is that these materials are like other PGEC materials, such as $CoSb_3$, because the main charge carrying network (Cu-Se) is differently bonded as compared to Sn, which acts as a "filler" atom that contributes to lattice thermal conductivity reduction. It is worth noting that Cu_2SnSe_3 was reported to undergo a structural transition from monoclinic to cubic upon substitution of In for Sn.[15]

The diamond-like compounds $Cu_2Ge_{1+x}Se_3$ are closely related to the $Cu_2CdSnSe_4$ and $Cu_2Sn_{1-x}In_xSe_3$ compounds, and we havd previously reported low κ and compositionally induced structural polymorphism in this system.[16] Here we report a systematic study on Ga-doped Cu_2GeSe_3 to try to optimize the electrical transport, and further we aim to understand the origin of low κ in these materials using elastic property measurements. Finally, we report a crystallographic polymorphic transition from orthorhombic to cubic that is caused by Ga doping.

EXPERIMENTAL DETAILS

$Cu_2Ga_xGe_{1-x}Se_3$ compounds for $0 \leq x \leq 0.1$ were synthesized by direct melting of Cu (99.9%, Alfa Aesar), Ga (99.99999%, Alfa Aesar), Ge (99.999%, Alfa Aesar), and Se (99.99%, Alfa Aesar). The stoichiometric mixtures of the elements were sealed in fused silica tubes under high vacuum, heated to 1273 K at a rate of 200 K/h, held at that temperature for 48 h, and then cooled to room temperature. To increase sample homogeneity and crystallinity, each sample was ground into powders, cold pressed into pellets, and annealed in evacuated fused silica tubes at 773 K for two weeks. The samples were reground and sintered in a hot press using a graphite die (diameter 12.7 mm) under dynamic vacuum and with the application of 50 MPa uniaxial pressure at 893 K. The relative densities of the consolidated samples were $\geq$ 95%.

Room temperature powder x-ray diffraction (XRD) data were collected on a Siemens D5000 diffractometer equipped with Cu K_α radiation (λ = 1.5418 Å) to check phase purity and identity. Quantitative elemental analyses of sintered $Cu_2Ga_xGe_{1-x}Se_3$ ($0 \le x \le 0.1$) samples were performed with a Cameca SX100 Electron Probe Micro Analyzer (EPMA) using an accelerating voltage of 25 keV and averaging 18 scans on each sample. The compositions based on the averaging of the 18 spots and their accompanying standard deviations are reported in Table I. Data for κ and S were collected from 3.5 K to 350 K on rectangular bar-shaped samples with dimensions ~2.5 mm × 2.8 mm × 6 mm using a Quantum Design Physical Property Measurement System (PPMS). Low temperature heat capacity (C_p) measurements were made on a 20 mg consolidated specimens using the PPMS with the heat capacity measurement option. The sample stage and mounting grease (Apiezon N-grease) were carefully characterized and stored in an addenda file, and then the sample was affixed with grease to the test fixture for measurement. The Debye temperatures (θ_D) were extracted from this data. Electrical resistivity and Hall effect measurements were made by a standard four-probe AC technique using a Linear Research AC resistance bridge and cryostat equipped with a 5 T magnet. Seebeck coefficient and resistivity measurements from 325 K to 745 K were performed by using an ULVAC ZEM-3 system. For thermal conductivity determination at high temperatures, we used the relation $\kappa = C_p \cdot D \cdot d$, where thermal diffusivity (D) was measured with an Anter FL5000 laser flash diffusivity instrument, high temperature specific heat (C_p) was determined by the ratio method with a sapphire reference using a Netzsch Differential Scanning Calorimetry 404c, and the sample density d was determined by total mass divided by its volume.

Resonant ultrasound spectroscopy (RUS) was performed on disk-shaped specimens to determine elastic modulus (E) and Poisson's ratio (υ). The disks were cut from hot pressed

polycrystalline ingots, and all measurements were performed in air inside a furnace while supported by ceramic waveguides attached to the RUS transducers. Resonant frequencies were then identified, and by knowing each specimen's density and dimensions, the modal analysis output from the finite element analysis software ANSYS was used to determine E and υ for each sample. Next, the shear (G) and bulk (B) moduli were calculated using the relations:

$$G = E/[2(1 + \upsilon)] \quad \text{and} \quad B = E/[3(1 - 2\upsilon)]. \tag{1}$$

The transverse (v_T), longitudinal (v_L) and mean (v_m) sound velocities were also extracted from the RUS data using the relations $v_T = E/d$ and $v_L = (E/d) \times [(1 - \upsilon)/((1 + \upsilon)(1 - 2\upsilon))]^{1/2}$. To obtain v_m, the geometric mean of the two transverse branches and the one longitudinal branch are computed. Due to the orthorhombic symmetry of the majority phase, the relationships between the different moduli are only approximate as they were derived for material with cubic symmetry, but due to the highly symmetric nature of these materials (i.e., the three-dimensional diamond-like tetrahedral bonding that leads to local cubic point symmetry instead of a structure with reduced dimensionality), the bulk and shear moduli and sound velocity estimates are reasonable. The coefficients of thermal expansion (CTE) were measured using a dual-rod dilatometer on specimens that were in the form of rectangular prismatic bars. A sapphire bar was cut to the nominal length of the specimens (~10 mm) and served as a standard. The sample bars were then heated in parallel with the sapphire bar in the dilatometer's tube furnace at a rate of 2 K/min to 423 K in flowing argon. Instantaneous elongations of both the specimen and sapphire standard were measured with linear variable differential transducers. The differences in elongation between the specimen and the sapphire standard were then used to calculate the specimens' CTEs as a function of temperature.

RESULTS AND DISCUSSION

The diamond-like compounds, based on the formula $Cu_2Ge_{1+x}Se_3$, are composed of a three-dimensional network of cations (Cu and Ge) tetrahedrally coordinated by Se anions, with Se anions likewise tetrahedrally coordinated by the cations. The stoichiometric parent compound Cu_2GeSe_3 ($A_2^{I}B^{IV}C_3^{VI}$) has four valence electrons per atom similar to other four-electron compounds that include the well-known semiconductors Ge, Si, and $A^{II}B^{VI}$ zincblende compounds. Based on the simple valence electron count, Ga substitution for Ge in Cu_2GeSe_3 should lead to p-type conduction because Ga has one fewer valence electron than Ge. Cu_2GeSe_3 crystallizes in an orthorhombic structure (space group *Imm*2), with lattice constants a = 11.86 Å, b = 3.96 Å, and c = 5.485 Å with crystallographically ordered cations and anions on their respective sites.[17] It has been further reported by several researchers that Cu_2GeSe_3 undergoes a phase transformation caused by site-exchange order/disorder near its melting temperature.[18] The high temperature phase is a disordered face centered cubic (fcc) structure (space group *F*-43*m*) and low temperature structure is the ordered orthorhombic *Imm2* phase. In addition, as the Ge content is increased in $Cu_2Ge_{1+x}Se_3$, a structural phase transition takes place resulting in conversion of the orthorhombic cell to the fcc structure with a unit cell parameter of ~ 5.55 Å. This transition corresponds to multiplying the *a*-axis of the orthorhombic cell by $\sqrt{2}/3$ and the *b* axis by the square root of 2. The *c*-axis remains the same in both structures aside from a small expansion. This means that new fcc unit cell axis is the hypotenuse of the right isosceles triangle defined by the orthorhombic *b*-axis. Figure 1 shows the geometric relationship between these two structures, where only the anion sublattice is shown for clarity. All cations and anions retain their tetrahedral coordination in the fcc structure, but due to the reduction in the unit cell volume

(255 Å^3 for the orthorhombic cell and 170 Å^3 for the cubic) and accompanying reduction in the asymmetric unit, the cations sites are crystallographicaly disordered in the fcc structure.

Figure 2 shows powder XRD data of $Cu_2Ga_xGe_{1-x}Se_3$ for $0 \leq x \leq 0.1$, which crystallizes in the orthorhombic Cu_2GeSe_3structure (space group *Imm*2), and all reflections are indexable to that phase for low Ga doping. With increased Ga doping levels, however, additional reflections at high diffraction angles are observed and are due to the presence of the fcc phase described above. Details of the growth of the reflections for the fcc phase are shown in the inset of Fig. 2. In contrast to undoped Cu_2GeSe_3, here we have a phase transition that is likely caused by Ga substitutional disorder rather than only site-exchange order/disorder or atomic disorder arising from insufficient or incomplete annealing. EPMA reveals an inhomogeneous Ga distribution in all Ga-doped samples, as shown in Fig. 3, and this inhomogeneity is also reflected in the large standard deviations reported for the Ga content in Table 1. These Ga rich regions are not secondary phases as PXRD reveals only the presences of the *Imm*2 and the *F*-43*m* structures, both of which are diamond like in nature. We speculate that the Ga-rich regions of the samples are the disordered fcc phase because the larger Ga atoms substituting for smaller Ge atoms could increase the cubicity of the atomic arrangement by reducing orthorhombic distortions of the lattice and thereby favor the more symmetric fcc lattice. Further support of our speculation that the more Ga rich regions are cubic is the fact that in the absence of Ga, or in small concentrations the phase crystallizes solely as the body centered orthorhombic. This result is also consistent with the observations of Sharma *et al*. that for the $Cu_2Ge_{1+x}Se_3$ ($0.1 \leq x \leq 0.55$) and $Cu_2GeSi_{0.5}Se_3$ systems, an increase in Ge content or the incorporation of Si into the orthorhombic phase favors the formation of the cubic structure.[19,20] This is not to say that the orthorhombic phase of the present study is devoid of Ga. EPMA results clearly reveal that Ga is distributed throughout the

entire material, only that the Ga distribution is not homogenous on a macroscopic scale. Back scattered electron images and secondary x-ray maps for all constituent elements for the $x = 0.1$ sample are shown in Fig. 3. The x-ray maps show that Cu and Se are homogenously distributed, while Ga and Ge are markedly inhomogeneous. It is also evident that, at least qualitatively, the compositions of Ga and Ge are correlated such that higher levels of Ga correspond to lower levels of Ge as expected for Ga substituting for Ge in the lattice. The nominal and actual compositions of all samples are summarized in Table 1 along with the other room temperature physical parameters discussed below.

Figure 4(a) shows the temperature dependence of ρ for $Cu_2Ga_xGe_{1-x}Se_3$ ($0 \leq x \leq 0.1$). Undoped Cu_2GeSe_3 exhibits typical semiconducting behavior with a high resistivity on the order of 10^2 and 10^3 mΩ cm that decreases with increasing temperature, except for a broad peak at room temperature. At room temperature, ρ decreases significantly with increased Ga doping from a value of 287 mΩ cm for Cu_2GeSe_3 to 0.95 mΩ cm for $Cu_2Ga_{0.1}Ge_{0.9}Se_3$. This result suggests that Ga is successfully substituted for Ge in this system and that Ga, which has the electron configuration $4s^2p^1$, is a good hole dopant (i.e., electron acceptor) when substituted for Ge, which has the electron configuration ($4s^2p^2$), if we assume a simple sp^3 hybridization valence bonding scheme. These conclusions are further supported by the Hall effect measurements presented below.

The Seebeck coefficients, S, of $Cu_2Ga_xGe_{1-x}Se_3$ ($0 \leq x \leq 0.1$) all have positive values over the entire temperature range studied, as shown in Figure 4(b), indicating that electrical conduction is dominated by p-type charge carriers. Undoped Cu_2GeSe_3 shows the largest value of $S = 446$ μV K^{-1} at 745 K, which is comparable to other p-type thermoelectric materials, such as Cu_2SnSe_3 and Cu_3SbSe_4.[21] With increasing Ga concentration, S decreases to 137 μV K^{-1} at

745 K for x = 0.1, as shown in Fig. 4(b). As the temperature is increased, S increases monotonically for all samples up to 745 K with the exception of undoped Cu_2GeSe_3, which exhibits a slight non-monotonic feature above about 450 K.

Figure 4(c) shows that (1) all samples have a low κ at room temperature, ranging from $\kappa = 2.8$ W m^{-1} K^{-1} for $Cu_2Ga_{0.1}Ge_{0.9}Se_3$ to κ = 1.7 W m^{-1} K^{-1} for Cu_2GeSe_3, and (2) as the temperature increases, κ decreases monotonically from its peak value at low temperature to a still decreasing value at 745 K. Values as low as κ = 0.67 W m^{-1} K^{-1} were observed for Cu_2GeSe_3 at 745 K, and this is comparable to values observed for state-of-the-art Bi-Te compounds where such low κ values can be attributed to complex, low symmetry crystal structures and heavy constituent elements. The diamond-like materials studied here, by contrast, have structures with lower complexity and higher symmetry than Bi_2Te_3 and contain relatively light constituent elements.

Figure 5(a) shows the carrier concentration (p), and Fig. 5(b) shows the Hall mobility (μ_H) as a function of temperature. Hall coefficients (R_H), listed in Table 1, are positive for all samples over the entire temperature range, which is indicative of p-type, or hole dominated electrical conduction, and this is consistent with the observed positive values of S. The carrier concentrations (p) were calculated from the Hall coefficients using $p = 1/R_H \cdot e$, where e is the fundamental charge. Undoped Cu_2GeSe_3 has a charge carrier concentration ~7.9×10^{17} cm^{-3} at room temperature, which is typical for lightly doped semiconductors. With increasing Ga doping, the room temperature charge carrier concentration increases to ~1.4×10^{21} cm^{-3} for $Cu_2Ga_{0.1}Ge_{0.9}Se_3$ and is nearly temperature independent, which is typical of heavily doped semiconductors.

The temperature dependence of the Hall mobility μ_H for each sample is shown in Fig. 5(b). Near room temperature Cu_2GeSe_3 displays an approximate $\mu_H \propto T^{-3/2}$ dependence, which is consistent with acoustic phonon scattering being the dominant charge carrier scattering mechanism. As the Ga doping level increases, however, μ_H becomes more weakly temperature-dependent, which implies a mixture of charge carrier scattering mechanisms including acoustic phonon, carrier-carrier, ionized impurity, and neutral impurity scattering. Room temperature values of ρ, κ, S, p, and μ_H are listed in Table 1.

As noted above, the total thermal conductivities of the samples presented here are as low as some Bi_2Te_3 based compounds that have highly complex crystal structures, substitutional and site-exchange disorder, and Van der Waals gaps, all of which contribute strongly to reducing the phonon mean free path and group velocity and thereby lower κ. While it is true that crystallographic disorder is present in the diamond-like materials discussed here, the highly symmetric nature of the crystal sub-structures and the comparatively small unit cell sizes make it somewhat surprising that they exhibit such low values of κ.

The total thermal conductivity κ is composed of an electronic portion (κ_e) and a lattice portion (κ_L) such that $\kappa = \kappa_e + \kappa_L$. The first term, κ_e, arises from heat transferred by charge carriers, and the second term, κ_L, arises from heat carried by phonons. κ_e can be computed from electrical resistivity using the Wiedemann-Franz law $\kappa_e = (L/\rho)T$, where the Lorenz number L is taken to be approximately $2.4 \times 10^{-8}\ V^{-2}K^2$. κ_L is determined by the dominant phonon scattering mechanisms that include: boundary, point defect, phonon-charge carrier, and phonon-phonon Umklapp scattering. At high temperatures, Umklapp scattering processes, by which crystal momentum is not conserved, become dominant. If one assumes that heat is conducted only by

acoustical phonons and that these phonons interact only by Umklapp processes, κ_L can be expressed as[22-25]

$$\kappa_L = A\frac{\bar{M}\theta_D{}^3\delta}{\gamma^2 n^{2/3}T}, \quad (2)$$

where $\bar{M}$ is the average mass of the atoms in the crystal, θ_D is the Debye temperature, δ is the volume per atom, γ is the high temperature limit of the acoustic phonon Grüneisen parameter, n is the number of atoms in the primitive unit cell, and A is a collective physical constant ($A \approx 3.1 \times 10^{-6}$ when κ_L is in W m^{-1} K^{-1}, $\bar{M}$ in amu, and δ in Å). All quantities in Eq. (2) are known or can be calculated from crystallographic data with the exception of γ and θ_D. We obtained θ_D from specific heat C_p measurements on $Cu_2Ga_{0.1}Ge_{0.9}Se_3$ and by exploiting the low temperature T^3 dependence of the specific heat, namely $C_v \propto (T/\theta_D)^3$, and results in θ_D = 180 K. In some cases, however, θ_D is temperature dependent, but this value for θ_D (obtained from low temperature data) agrees well with values extracted from the heat capacity measurement over the entire temperature range of 2 K to 350 K. The specific heat C_p as a function of temperature is shown in Figure 6. The difference in the values of the isochoric specific heat (C_v) and the isobaric value (C_p) is expected to be very small, and we therefore assumed $C_p \approx C_v$ for this analysis.

To obtain values for γ, the elastic properties such as the bulk modulus (B) and the volumetric thermal expansion coefficient must be measured. The elastic, or Young's modulus (E) and Poisson's ratio (υ) can be determined by resonant ultra sound spectroscopy (RUS) whereby sound waves of varying frequencies are introduced into a sample of known dimension and density. Taking advantage of the intrinsic resonance of the sample, the values for E and υ can be extracted from the measured resonance frequencies. Measurements were performed on polycrystalline samples, so it is not possible to extract the directional dependence of the different

moduli, and this is particularly true for an orthorhombic system. Therefore, the values presented here are considered to be directionally averaged estimates. Because the bonding environments of the constituent atoms are highly symmetric in the diamond-like materials, (i.e., they are not layered compounds or otherwise have characteristics of low dimensional solids), the anisotropy of the moduli values will very likely be small.

From Young's modulus and Poisson's ratio, the bulk and shear moduli can be calculated from Eq. (1). Table 2 lists the room temperature values of Young's modulus (E) , Poisson's ratio (υ), and the calculated values of the shear (G) and bulk (B) moduli for all samples, and there is no clear trend in the values of these various moduli with Ga content. It is known that microstructural details can influence these properties, and the scatter in their values may be a result of differing amounts of porosity or cracks within each specimen. The relative density of $Cu_2Ga_{0.03}Ge_{0.97}Se_3$, for example, is the smallest among the samples and it also has a significantly lower value for the three moduli measured.

The high temperature limit of the acoustic phonon Grüneisen parameter γ, which is a measure of the bonding anharmonicity, is defined as[26]

$$\gamma = \frac{3\beta B V_m}{C_V}, \tag{3}$$

where β is the volume thermal expansion coefficient, B is the isothermal bulk modulus, V_m is the molar volume, and C_v is the isochoric specific heat per mole. The volume thermal expansion coefficient was taken to be a factor of three times the linear CTE, as measured using the dilatometer measurements, yielding a value of $\beta = 26.6 \times 10^{-6}$ K^{-1} for all samples measured. The isothermal bulk modulus of $Cu_2Ga_{0.1}Ge_{0.9}Se_3$ was determined to be B = 38.7 GPa, and the heat capacity measurements gave a room temperature value of $C_v \approx C_p$ = 0.34 J g^{-1} K^{-1}. Using these values in Eq. (3), γ was calculated to be 1.7 for $Cu_2Ga_{0.1}Ge_{0.9}Se_3$, which is a fairly large value for

a compound with a diamond-like structure. While this value was computed for only one composition, due to the similarity in the magnitude of the values needed to calculate this parameter (B, β, and V_m) among all the other samples it can be assumed that the large γ value is a common feature of these compounds. This value is comparable to $\gamma \approx 2.05$ for $AgSbTe_2$ and even higher than $\gamma \approx 1.45$ for PbTe.[27,28] Using Eq. (2) and all of the values of the physical parameters that we have determined from our measurements, we calculate a lattice thermal conductivity of κ_L ~2.0 W m^{-1} K^{-1} at 300 K. This is in good agreement with the experimental value of 2.16 W m^{-1} K^{-1} at 300 K we measured directly for $Cu_2Ga_{0.1}Ge_{0.9}Se_3$.

Low thermal conductivity is not generally expected for such highly symmetric diamond-like compounds. One example is ZnSe which has the parent structure type (zincblende) for the $Cu_2Ga_xGe_{1-x}Se_3$ compounds; its thermal conductivity is κ = 18 W m^{-1} K^{-1} at 300 K, and we expect that this large value is due to a combination of a high crystal symmetry, a lack of crystallographic disorder, a small unit cell volume, and a low Grüneisen parameter of $\gamma \sim 0.7$.[29] The large γ value of PbTe is likely due to octahedral atomic coordination in the NaCl-type or rocksalt crystal structure, and such a high coordination number and the associated high anharmonicity result in rather low values of κ_L.[30, 31] This behavior was recently explained more fully in terms of local structural distortions in PbTe which is close to a ferroelectric phase transition, thus resulting in bonding anharomonicity.[32]

In the case of $AgSbTe_2$, γ values even larger than that of PbTe have been explained by Morelli *et al.*[25] in terms of bonding anharmonicity caused by the additional non-bonding character of *s* valence electrons and part of the *p* valence electrons arising from Sb^{3+} ions. These non-bonding electrons can cause nonlinear repulsive forces resulting in anharmonicity. This result explains κ values that approach their minimum values even at low temperature for

$AgSbTe_2$. Finally, an exceptionally low thermal conductivity for Cu_3SbSe_3 arising from anharmonicity due to non-bonding electrons of Sb^{3+} ions has also been reported by Morelli *et al.* to support their previous hypothesis for $AgSbTe_2$.[33] In contrast to the above cases, the diamond-like Cu_2GeSe_3 system has a tetrahedrally coordinated bond scheme, which means, simplistically, that all valence electrons of the constituent atoms participate in sp^3 hybridization, thus no non-bonding interactions and the structure also possesses low coordination number for the atoms.

As explained above, the Cu_2GeSe_3 system has a quite interesting intrinsic structural feature arising from the substitutional disorder and size mismatch of constituent atoms. As shown in Fig. 1, the orthorhombic structure of Cu_2GeSe_3 can be viewed as a distortion of the parent cubic zincblende structure. The Ga-rich and Ga-poor regions may correspond to the fcc and orthorhombic structures, respectively and lead to a compositionally-induced structural modulation throughout the sample. It is believed that the Cu_2GeSe_3 system posses an intrinsic structural instability resulting in its low thermal conductivity as shown in Figure 4 and by Ga-doping further structural modulation in this system becomes identifiable from the PXRD in the inset of Figure 2.

The source of the large bonding anharmonicity in these materials in not entirely clear, but may be linked to the fact that these materials can undergo a compositionally or thermally induced phase transition with minimal perturbation and that there is an intrinsic anharmoncity associated with this structural instability due to localized distortion of bonds like that described for PbTe.[32] Recent ab-initio phonon dispersion calculations performed for PbTe find a transverse optical (TO) phonon mode instability at the Brillouin zone center which would break the crystallographic inversion center resulting in the predicted ferroelectric transition. This phonon mode was found to be soft and highly anharmonic. While TO modes are not associated

with the ability to carry large amounts of heat, the calculations further show a strong coupling between the TO modes and the longitudinal acoustical (LA) modes imparting the stronger phonon scattering of anharmonicity to the LA branches which do carry most of the heat. While this result for PbTe is for a para- to ferroelectric transition it maybe that this concept is more general and that provided there is a path for coupling between TO modes associated with any structural distortion or near crystallographic structural transitions (TO instabilities away from centers of inversion) and heat carrying LA modes that the anharmonicity can be imparted to the LA modes resulting in shorter phonon scattering times and lower κ_L. It is thought that such a mechanism may be present in Cu_2GeSe_3 and the related Ga doped samples presented here.

Figure 7 shows the lattice thermal conductivity of $Cu_2Ga_{0.1}Ge_{0.9}Se_3$ as a function of temperature. The minimum lattice thermal conductivity κ_{Lmin} can be estimated from kinetic theory using:

$$\kappa_L = \frac{1}{3} C_v v_m l, \tag{3}$$

where C_v is heat capacity, v_m the mean sound velocity, and l the mean free path of phonons. The mean sound velocities that were extracted from the elastic property measurements as described in the experimental details section, listed in Table 2, do not show much variation with Ga content. If we assume the minimum l to be the interatomic distance of ~2.3 Å for $Cu_2Ga_{0.1}Ge_{0.9}Se_3$, then Eq. (3) gives $\kappa_{Lmin.} = 0.6$ $Wm^{-1}K^{-1}$. Alternatively, the minimum lattice thermal conductivity can be calculated from the model of Cahill and Pohl, the minimum thermal conductivity for such a model can be expressed as

$$\kappa_{Lmin} = \frac{1}{2.48} k_B n^{\frac{2}{3}} (2v_t + v_l) \tag{4}$$

where n is the number of atoms in the asymmetric unit and v_t and v_l are the transverse and longitudinal sound velocities respectively and k_B is Boltzmann's constant. This analysis leads to a $\kappa_{Lmin} = 0.7$ W m^{-1} K^{-1} for the same sample.[35]

At high temperatures, the measured lattice thermal conductivity for $Cu_2Ga_{0.1}Ge_{0.9}Se_3$ approaches this theoretical minimum value κ_{Lmin} as shown in Fig. 7. It is worth noting that the thermal conductivities observed for $Cu_2Ga_xGe_{1-x}Se_3$ are even lower than those reported for the In/Sn analogs ($Cu_2In_xSn_{1-x}Se_3$) despite being composed of lighter elements with a much smaller mass contrast on the mixed cation site of the higher symmetry polymorph (Cu and Ge vs. Cu and Sn). One may expect that if this site occupancy mixing (defect scattering) were the dominant phonon scattering mode that the trend we observed would be reversed as larger mass contrast leads to larger mass fluctuation scattering parameter.[36] Though this type of point defect scattering generally only effectively scatters short wave length phonons.

The dimensionless figure of merit ZT as a function of temperature is shown in Fig. 8, and the highest value of $ZT = 0.5$ was found for $Cu_2Ga_{0.07}Ge_{0.93}Se_3$ at 745 K. This value of ZT is about a 60 % enhancement compared to undoped Cu_2GeSe_3 and is comparable to the results for the quaternary Cu-doped $Cu_2CdZnSe_4$ and Cu_2ZnSnX_4 (X = S, Se).[11-13]

SUMMARY

We have prepared a series of Ga doped diamond-like materials with the general formula $Cu_2Ga_xGe_{1-x}Se_3$ and have evaluated their transport and elastic properties. From transport measurements and EPMA data, we conclude that Ga was successfully incorporated into the structure by substituting for Ge and thereby is a p-type dopant. As the Ga doping level is increased in the orthorhombic Cu_2GeSe_3 structure, the compound undergoes a structural

transition to a cubic phase perhaps due to the larger atomic radius of Ga compared to Ge. At high Ga content, the samples show both the orthorhombic and cubic structures in powder x-ray diffraction patterns. The intrinsic propensity of Cu_2GeSe_3 to undergo such a transition together with the accompanying compositional disorder is one possible explanation of the large bond anharmonicity characterized by large high temperature acoustical phonon Grüneisen parameter γ that we observed for this system, analogous to that described for PbTe by An, et. al.[34].

The presence of large anhamonicity, which we infer from the magnitude of the Grüneisen parameter, gives rise to enhanced scattering of the heat carrying phonons and ultimately a much diminished thermal conductivity. The sample with the highest level of Ga doping approaches its theoretical minimum value of lattice thermal conductivity at temperatures between 700 K and 750 K. In the present case, however, the power factor S^2/ρ is quite low for these materials due to very low carrier mobility. Consequently, only modest values of $ZT = 0.5$ at 750 K were obtained despite the fact that these materials have very low thermal conductivity.

ACKNOWLEDGMENTS

The work is supported by GM and by DOE under corporate agreement DE-FC26-04NT42278. Elemental analysis was provided by Richard Waldo, and powder x-ray diffraction measurements were performed by Richard Speer, Jr. is highly appreciated. The work at the University of Michigan is supported as part of the Revolutionary Materials for Solid State Energy Conversion, an Energy Frontier Research Center funded by the U.S. Department of Energy, Office of Basic Energy Sciences under Award Number DE-SC0001054.

REFERENCES

1. J. Yang and T. Caillat, MRS Bull. **31**, 224 (2006).
2. F. J. DiSalvo, Science **285**, 703 (1999).
3. G. J. Snyder and E. S. Toberer, Nat. Mater. **7**, 105 (2008).
4. B. C. Sales, D. Mandrus, and R. K. Williams, Science **272**, 1325 (1996).
5. V. Keppens, D. Mandrus, B. C. Sales, B. C. Chakoumakos, P. Dai, R. Coldea, M. B. Maple, D. A. Gajewski, E. J. Freeman, and S. Bennington, Nature **395**, 876 (1998).
6. J. Yang, W. Zhang, S. G. Bai, Z. Mei, and L. D. Chen, Appl. Phys. Lett. **90**, 192111 (2007).
7. K. F. Hsu, S. Loo, F. Guo, W. Chen, J. S. Dyck, C. Uher, T. Hogan, E. K. Polychroniadis, and M. G. Kanatzidis, Science **303**, 818 (2004).
8. B. Poudel, Q. Hao, Y. Ma, Y. Lan, A. Minnich, B. Yu, X. Yan, D. Wang, A. Muto, D. Vashaee, X. Chen, J. Liu, M. S. Dresselhaus, G. Chen, and Z. Ren, Science **320**, 634 (2008).
9. G. J. Snyder, M. Christensen, E. Nishibori, T. Caillat, and B. B. Iversen, Nat. Mater. **3**, 458 (2004).
10. E. S. Toberer, A. F. May, and G. F. Snyder, Chem. Mater. **22**, 624 (2010).
11. M. L. Liu, I. W. Chen, F. Q. Huang, and L. D. Chen, Adv. Mater. **21**, 1 (2009).
12. M. L. Liu, F. G. Huang, L. D. Chen, and I. W. Chen, Appl. Phys. Lett. **94**, 202103 (2009).
13. X. Y. Shi, F. Q. Huang, M. L. Liu, and L. D. Chen, Appl. Phys. Lett. **94**, 122103 (2009).
14. C. Sevik and T. Çağin, Appl. Phys. Lett. **95**, 112105 (2009).
15. X. Shi, L. Xi, J. Fan W. Zhang, and L.D. Chen. Chem. Mater. DOI 10.1021/cm101589c
16. J. Y. Cho, X. Shi, J. R. Salvador, J. Yang, and H. Wang, J. Appl. Phys. **108**, 1 (2010).
17. E. Parthé and J. Garin, Monatsh. Chem. **102**, 1197 (1971).
18. L. I. Berger and V. D. Prochukhan, Ternary Diamond-like Semiconductors (Consultants

Bureau, New York, 1969), p. 47.

19. B. B. Sharma and H. Singh, J. Solid State Chem. **11**, 285 (1974).
20. B. B. Sharma, R. Ayyar, and H. Singh, Phys. Status Solidi **29**, K17 (1975).
21. D. T. Morelli and E. J. Skoug, Mater. Res. Soc. Symp. Proc. **1166**, N06-07 (2009).
22. G. Leibfried and E. Schlömann, Nachrichten der Akademie der Wissenschaften in Göttingen **4**, 71 (1954).
23. G. A. Slack, Solid State Phys. Adv. Res. Appl. **34**, 1 (1979).
24. D. T. Morelli and J. P. Heremans, Appl. Phys. Lett. **81**, 5126 (2002).
25. D. T. Morelli, V. Jovovic, and J. P. Heremans, Phys. Rev. Lett. **101**, 035901 (2008).
26. S. Ganesan, Philos. Mag. **7**, 197 (1962).
27. *Physics of non-tetrahedrally bonded binary compounds II*, Landolt-Börnstein Numerical Data and Functional Relationships in Science and Technology, Group III, Vol. 17, Subvol. F, (Springer, Berlin, 1983), p. 419, Fig. 18.
28. G. A. Slack, in *Solid State Physics*, edited by H. Ehrenreich, F. Weitz, and D. Turnbull (Academic Press, New York, 1979), Vol. 34, pp. 1-71.
29. *Physics of II-VI and I-VII Compounds, Semimagnetic Semiconductors*, Landolt-Börnstein Numerical Data and Functional Relationships in Science and Technology, Group III, Vol. 17, Subvol. B, (Springer, Berlin, 1982), p. 397, Fig. 39.
30. A. F. Ioffe, *Physics of Semiconductors*, (Infosearch, London, 1958).
31. D. T. Morelli and G. A. Slack, *in High Thermal Conductivity Materials*, edited by S. Shinde and J. Goela (Springer, New York, 2005), p. 37.
32. E. S. Bozin, C. D. Malliakas, P. Souvatzis, T. Proffen, N.A. Spaldin, M.G. Kanatzidis and S. J. L. Billinge, Science, **330**, 1660 (2010).

33. E. J. Skoug, J. D. Cain, and D. T. Morelli, Appl. Phys. Lett. **96**, 181905 (2010).

34. J. An, A. Subedi, and D.J. Singh, Solid State Comm. **148**, 417 (2008).

35. Cahill, D. G.; Pohl, R. O. *Ann. Rev. Phys. Chem.* **1988**, 39, 93

36. B. Abeles, Phys Rev. **131** 1906 (1963).

Table 1. Nominal and Actual Composition, and room temperature values of the Electrical Resistivity (ρ), Thermal Conductivity (κ), Seebeck coefficient (S), Carrier concentration (p), and Mobility (μ_H) for $Cu_2Ga_xGe_{1-x}Se_3$.

Nominal Composition	Actual Composition*	ρ (mΩ cm)	κ (W/m K)	S (μV/K)	$p \times 10^{20}$ (cm^{-3})	μ_H (cm^2/V s)
Cu_2GeSe_3	$Cu_{2.00(1)}Ge_{0.96(1)}Se_{2.82(1)}$	287	1.9	330	0.000787	27.64
$Cu_2Ga_{0.01}Ge_{0.99}Se_3$	$Cu_{2.00(1)}Ga_{0.01(1)}Ge_{0.94(1)}Se_{2.80(1)}$	9.02	2.2	152	0.95	7.28
$Cu_2Ga_{0.03}Ge_{0.97}Se_3$	$Cu_{2.00(1)}Ga_{0.03(1)}Ge_{0.91(2)}Se_{2.80(1)}$	4.07	1.7	66	4.61	3.33
$Cu_2Ga_{0.05}Ge_{0.95}Se_3$	$Cu_{2.00(2)}Ga_{0.05(2)}Ge_{0.91(2)}Se_{2.83(2)}$	2.07	2.3	60	10.1	3.00
$Cu_2Ga_{0.07}Ge_{0.93}Se_3$	$Cu_{2.00(2)}Ga_{0.07(3)}Ge_{0.90(3)}Se_{2.85(1)}$	1.32	2.2	54	10.8	4.37
$Cu_2Ga_{0.1}Ge_{0.9}Se_3$	$Cu_{2.00(2)}Ga_{0.10(3)}Ge_{0.86(2)}Se_{2.81(2)}$	0.95	2.8	51	13.7	4.80

*Actual Compositions were determined by EPMA and normalized to copper.

Table 2. Room temperature values of the Young's Modulus (E), Poison's Ratio (υ), Shear Modulus (G), Bulk Modulus (B), Longitudinal Sound Velocity (v_L), Transverse Sound Velocity (v_T), Mean Sound Velocity (v_m), and Volume Thermal Expansion Coefficient for $Cu_2Ga_xGe_{1-x}Se_3$.

Sample	E (GPa)	Y	G (GPa)	B (GPa)	v_L (10^3 m/s)	v_T (10^3 m/s)	v_m (10^3 m/s)	Thermal Expansion Coefficient (10^{-6}/K)
$Cu_2Ga_{0.01}Ge_{0.99}Se_3$	63.5	0.22	26.0	38.2	3.65	2.18	2.41	26.6
$Cu_2Ga_{0.03}Ge_{0.97}Se_3$	45.6	0.22	18.6	27.4	3.19	1.91	2.11	26.6
$Cu_2Ga_{0.05}Ge_{0.95}Se_3$	56.7	0.22	23.2	34.1	3.50	2.09	2.31	26.6
$Cu_2Ga_{0.07}Ge_{0.93}Se_3$	49.6	0.24	20.0	31.8	3.34	1.95	2.16	26.6
$Cu_2Ga_{0.1}Ge_{0.9}Se_3$	53.5	0.27	21.1	38.7	3.53	1.98	2.21	26.6

Figure Captions

Figure 1. Depiction of the relationship between the diamond-like orthorhombic *Imm*2 and face centered cubic *F*-43*m* structures observed for $Cu_2Ga_xGe_{1-x}Se_3$. Black spheres are Se atoms, and cations were omitted for clarity.

Figure 2. Powder x-ray diffraction patterns of $Cu_2Ga_xGe_{1-x}Se_3$ for $0 \leq x \leq 0.1$ showing the appearance and increasing amount of a secondary phase as the Ga content is increased. The two peaks shown in the inset for a low Ga content near $2\theta = 55$ are the (321) and (013) reflections from the orthorhombic phase. As the Ga content reaches 0.07, a prominent reflection indexable as the (113) reflection of the face centered cubic polymorph of $Cu_2Ga_xGe_{1-x}Se_3$ appears and is a coalescence of the two corresponding reflections of the orthorhombic phase.

Figure 3. EPMA data for $Cu_2Ga_{0.1}Ge_{0.9}Se_3$ showing the back scattered electron image (a) and filtered secondary x-ray maps for Ga (b), Se (c), Cu (d), and Ge (e). All images were captured on the same specimen location, and the color variation indicates the composition variation of each element.

Figure 4. Temperature dependence of the electrical resistivity (a), Seebeck coefficient (b), and thermal conductivity (c) for $Cu_2Ga_xGe_{1-x}Se_3$.

Figure 5. Temperature dependence of the carrier concentration (a) and the Hall mobility (b) for $Cu_2Ga_xGe_{1-x}Se_3$.

Figure 6. Temperature dependence of the specific heat C_p for $Cu_2Ga_{0.1}Ge_{0.9}Se_3$.

Figure 7. Temperature dependence of lattice thermal conductivity of $Cu_2Ga_{0.1}Ge_{0.9}Se_3$. The solid line is the theoretical minimum lattice thermal conductivity calculated according to Eq. (3).

Figure 8. Temperature dependence of the figure of merit *ZT* for $Cu_2Ga_xGe_{1-x}Se_3$.

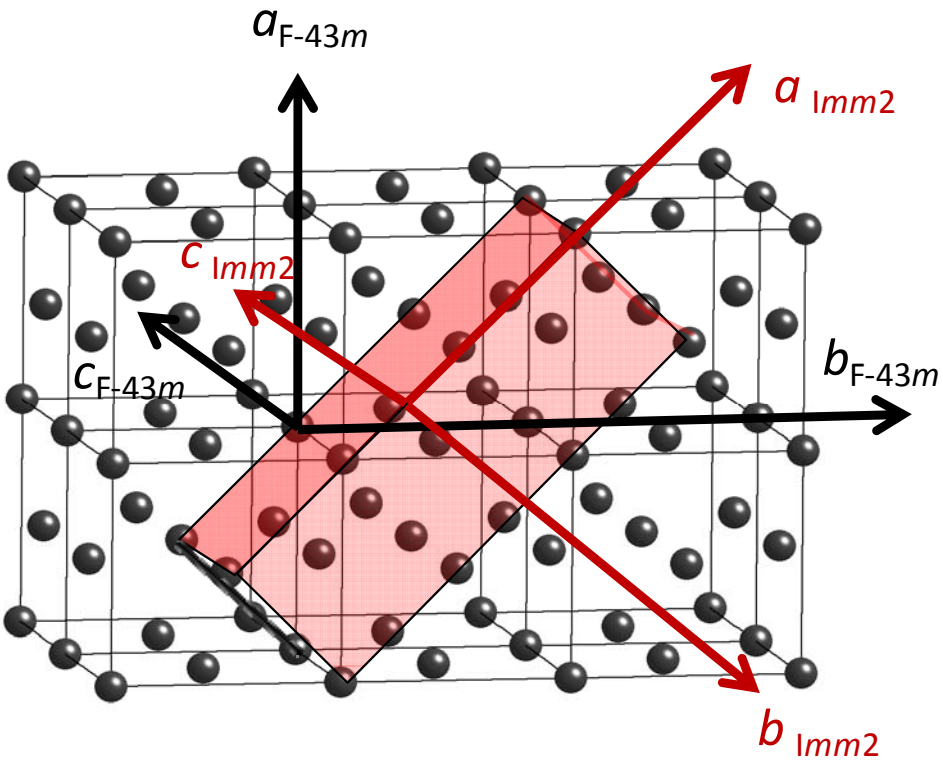

Figure 1.

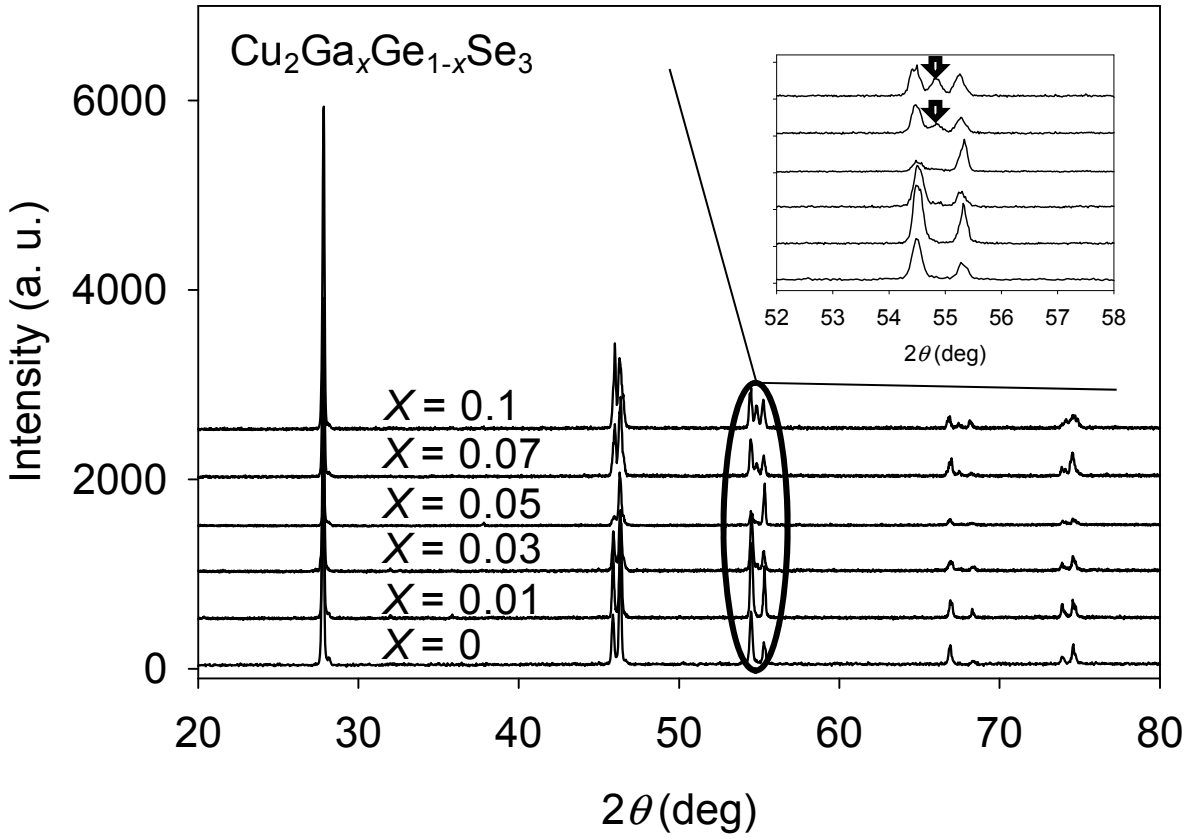
Cu2GaxGe1-xSe3
Intensity (a. u.)
6000
4000
2000
0
X = 0.1
X = 0.07
X = 0.05
X = 0.03
X = 0.01
X = 0
20
30
40
50
60
70
80
2θ (deg)
52
53
54
55
56
57
58
2θ (deg)

Figure 2.

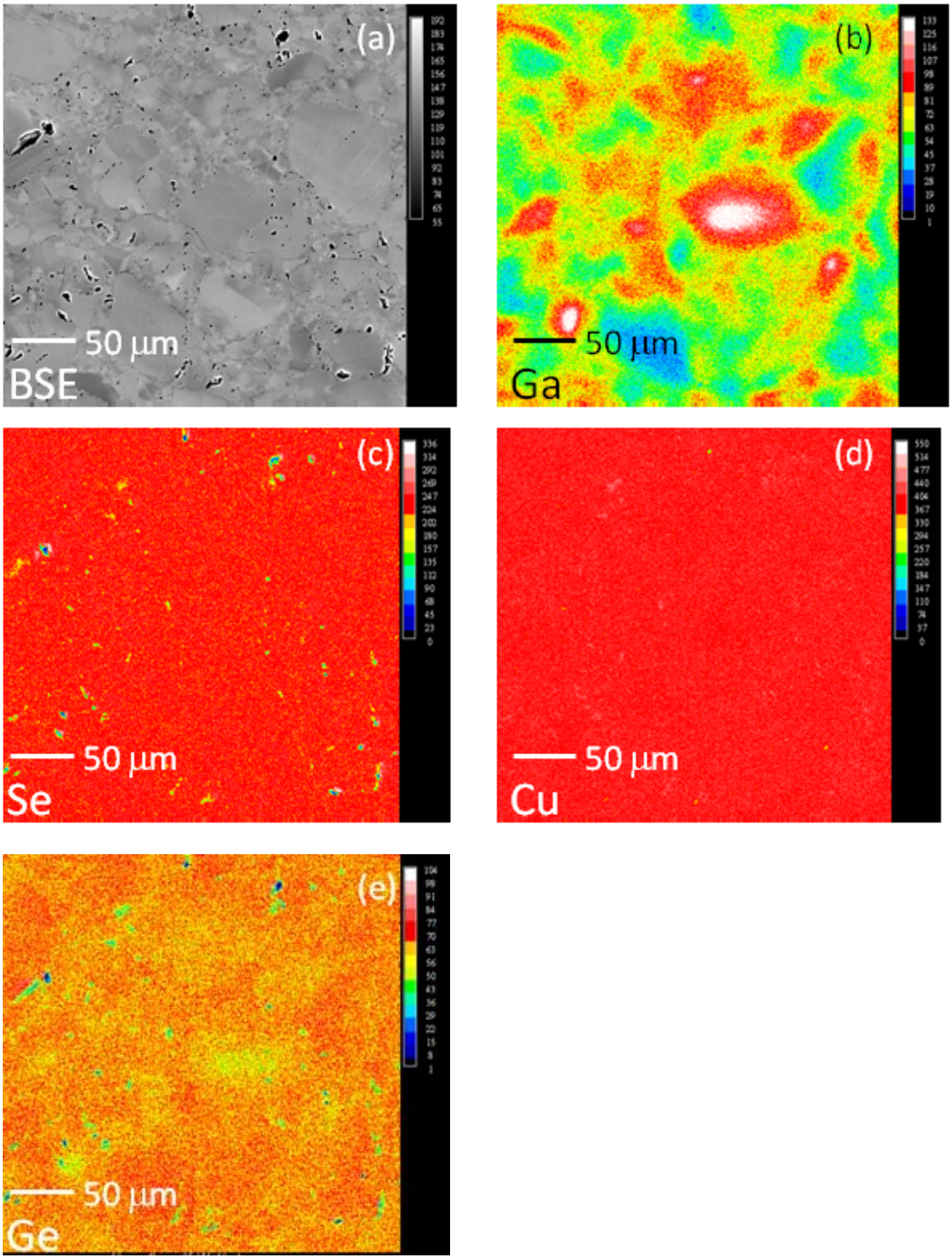

Figure 3.

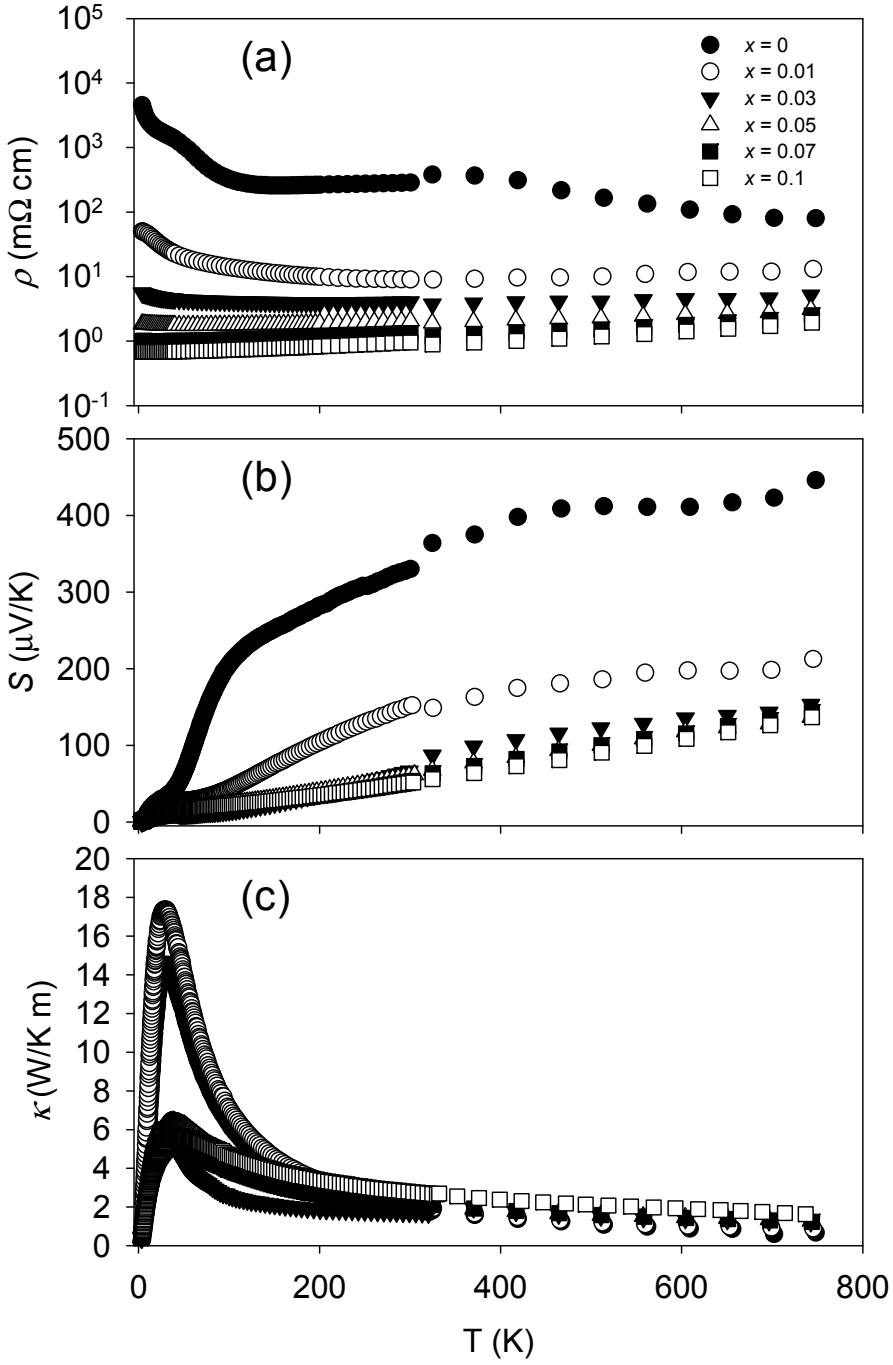

Figure 4.

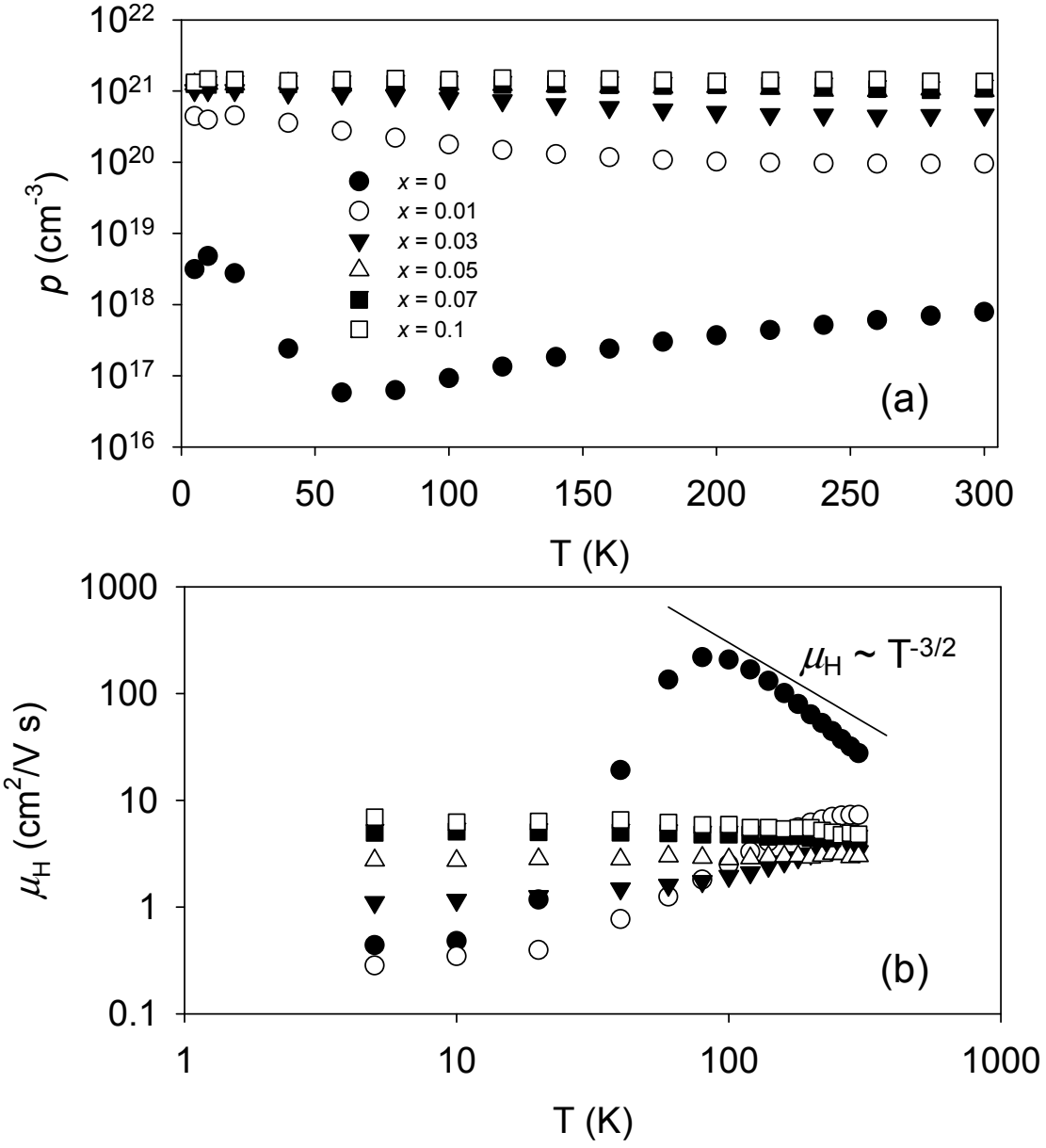
10^{22}
10^{21}
10^{20}
10^{19}
10^{18}
10^{17}
10^{16}
p (cm^{-3})
x = 0
x = 0.01
x = 0.03
x = 0.05
x = 0.07
x = 0.1
(a)
0
50
100
150
200
250
300
T (K)
1000
100
10
1
0.1
μ_H (cm^2/V s)
$\mu_H \sim T^{-3/2}$
(b)
1
10
100
1000
T (K)

Figure 5.

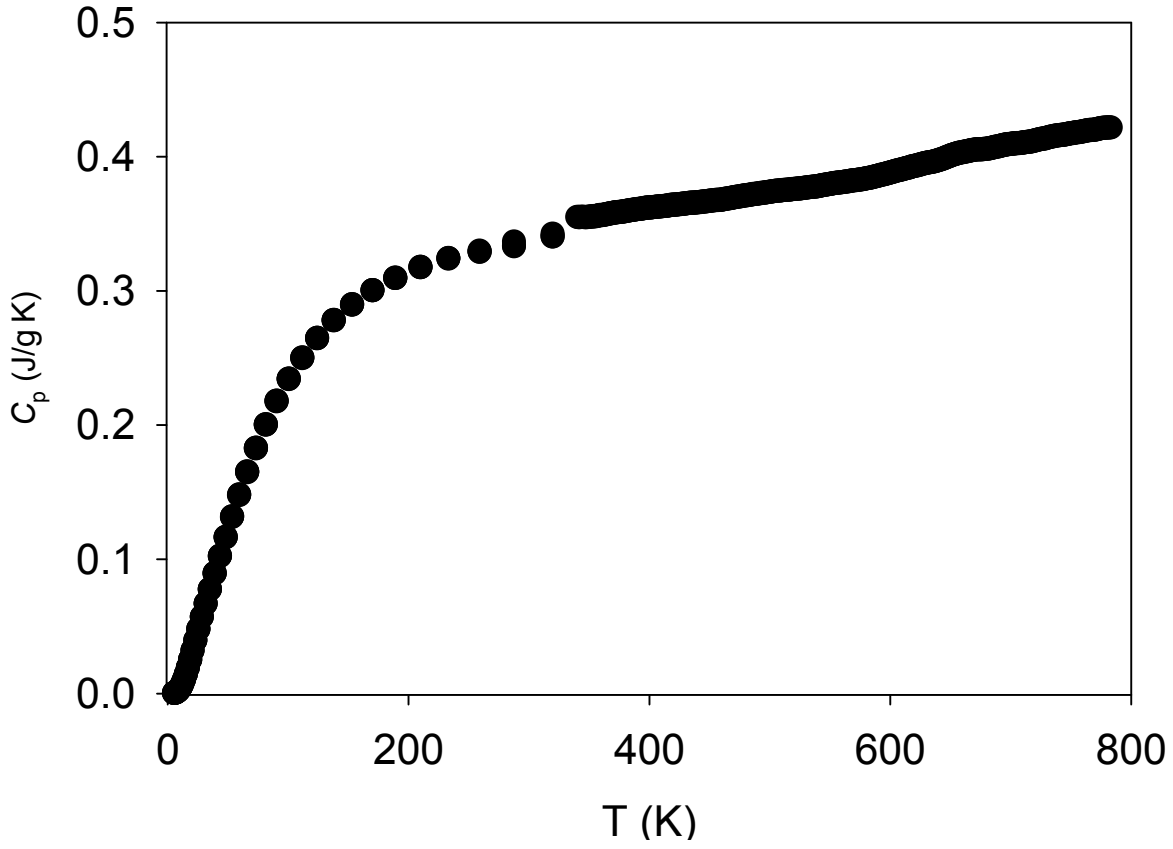

Figure 6.

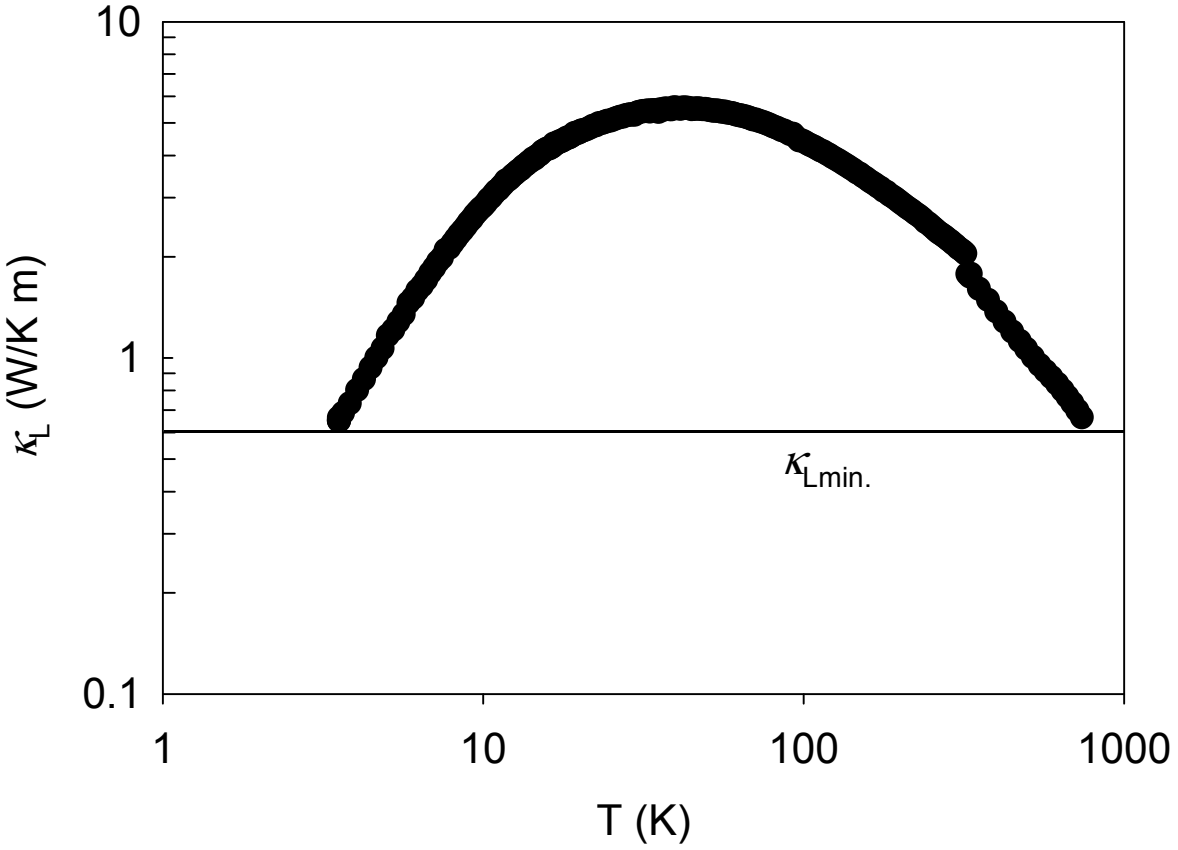

Figure 7.

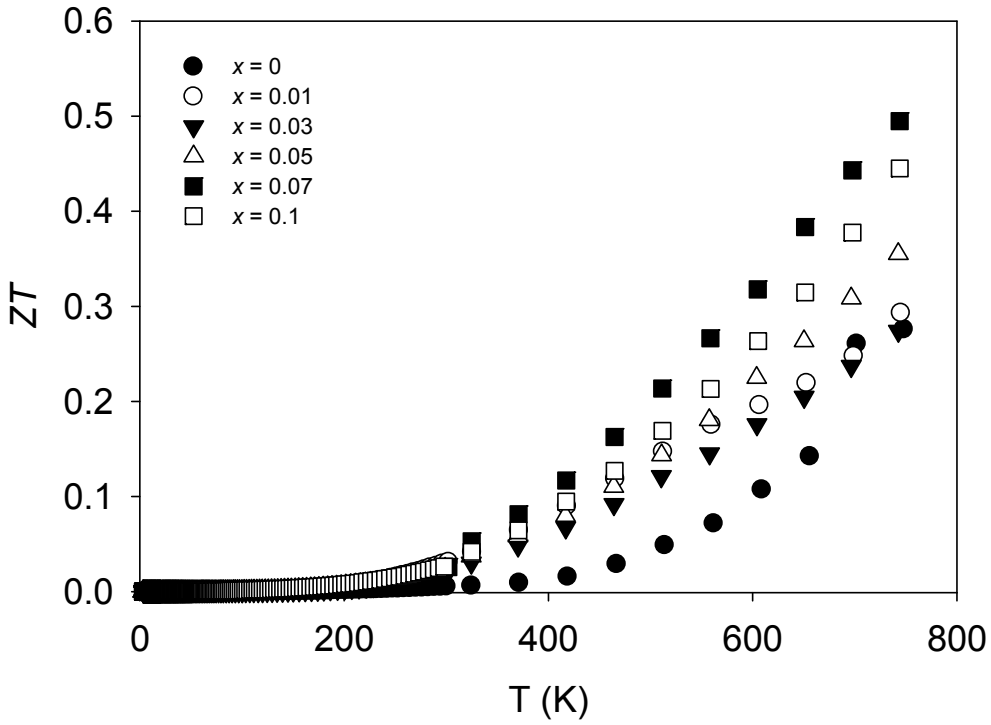
0.6
0.5
0.4
0.3
0.2
0.1
0.0
ZT
0
200
400
600
800
T (K)
x = 0
x = 0.01
x = 0.03
x = 0.05
x = 0.07
x = 0.1

Figure 8.